FULL PAPER

A Multi-Gradient Targeting Drug Delivery System Based on RGD-L-TRAIL-Labeled Magnetic Microbubbles for Cancer Theranostics

Lei Duan, Fang Yang, Wen He, Lina Song, Fan Qiu, Ning Xu, Lu Xu, Yu Zhang, Zichun Hua,* and Ning Gu*

The accurately and efficiently targeted delivery of therapeutic/diagnostic agents into tumor areas in a controllable fashion remains a big challenge. Here, a novel cancer targeting magnetic microbubble is elaborately fabricated. First, the γ-Fe$_2$O$_3$ magnetic iron oxide nanoparticles are optimized to chemically conjugate on the surface of polymer microbubbles. Then, arginine-glycine-aspartic acid-L-tumor necrosis factor-related apoptosis-inducing ligand (RGD-L-TRAIL), antitumor targeting fusion protein, is precisely conjugated with magnetic nanoparticles of microbubbles to construct RGD molecularly targeted magnetic microbubble, which is defined as RGD-L-TRAIL@MMBs. Such RGD-L-TRAIL@MMBs is endowed with the multigradient cascade targeting ability following by magnetic targeting, RGD, as well as enhanced permeability and retention effect regulated targeting to result in high cancerous tissue targeting efficiency. Due to the highly specific accumulation of RGD-L-TRAIL@MMBs in the tumor, the accurate diagnostic information of tumor can be obtained by dual ultrasound and magnetic resonance imaging. After imaging, the TRAIL molecules as anticancer agent also get right into the cancer cells by nanoparticle- and RGD-mediated endocytosis to effectively induce the tumor cell apoptosis. Therefore, RGD-L-TRAIL conjugated magnetic microbubbles could be developed as a molecularly targeted multimodality imaging delivery system with the addition of chemotherapeutic cargoes to improve cancer diagnosis and therapy.

L. Duan, Prof. F. Yang, W. He, L. Song,
Prof. Y. Zhang, Prof. N. Gu
State Key Laboratory of Bioelectronics
Jiangsu Key Laboratory for
Biomaterials and Devices
School of Biological Science
and Medical Engineering
Southeast University
Nanjing 210096, P. R. China
E-mail: guning@seu.edu.cn
L. Duan, Dr. N. Xu, Dr. L. Xu
School of Basic Medical Sciences
Nanjing Medical University
Nanjing 210029, P. R. China
Dr. F. Qiu, Prof. Z. Hua
State Key Lab of Pharmaceutical Biotechnology
School of Life Sciences
Nanjing University
Nanjing 210023, P. R. China
E-mail: huazc@nju.edu.cn

DOI: 10.1002/adfm.201603637

1. Introduction

In recent years, although significant achievement has been made in the field of cancer diagnosis and therapy, it is still imperfect due to the unsatisfactory diagnostic accuracy and low cancerous targeting therapy effect. Therefore, how to facilitate targeted delivery of specific therapeutic/diagnostic agents into tumor areas remains a big challenge. In the last decades, considerable attentions have been attracted by the development of innovative all-in-one drug delivery systems, which is characterized by several functionalities where both therapeutic and imaging components, and also targeting moieties, can be attached for simultaneous targeted therapy and imaging.[1,2] Based on this principle, various kinds of carriers such as dendrimers, vesicles, micelles, core–shell nanoparticles, microbubbles (MBs), liposomes, nanoemulsions, metals and metal oxides, as well as carbon nanotubes have been formulated as adjustable multifunctional formulations to target a specific site and generate imaging detectable signal for both diagnostic and therapeutic purposes.[3–10] Nevertheless, how to design a well-defined drug delivery system to achieve a high targeting specificity and delivery efficiency, while avoiding nonspecific binding is still lacking and remains highly desirable. Gas-filled MBs encapsulated with the polymer, lipid, or surfactant shells have been well established as the most effective ultrasound imaging contrast agent. Based on the multifunctional feasibility, microbubbles nowadays can be designed to combine with nanoparticles (such as iron oxide nanoparticles, gold and silver nanoparticles, quantum dots, etc.) to generate multimodal contrast agents,[11–16] or loaded with the drug, gene, and protein to constitute a multifunctional carrier material to deliver the therapeutic agents.[17–24] Although more accurate diagnosis is enabled with the assistance of microbubbles, it remains only blood pool images not the tissue penetrated images. Therefore, it is required the more elaborate fabrication of the molecularly targeted microbubbles to realize some give and take between imaging sensitivity, accuracy of molecular targeting, and controlled drug release.[25,26] In preliminary experiments, we have

prepared magnetic MBs with superparamagnetic iron oxide (SPIO) coated on the surface.[27] It is found that SPIO-coated MBs had good SPIO-carrying capacity, high magnetism, and strong and adjustable ultrasound (US)/magnetic resonance imaging (MRI) enhancement capability.[28]

Based on the feasibility of SPIO surface modification of the magnetic microbubbles (MMBs), in this study, molecularly targeted microbubbles for cancer theranostics were elaborately prepared by conjugating the arginine-glycine-aspartic acid (RGD)-L-tumor necrosis factor-related apoptosis-inducing ligand (RGD-L-TRAIL) protein on the surface of SPIO-loaded magnetic microbubbles. RGD-L-TRAIL is a fusion protein that can simultaneously target and kill tumor cells by binding to integrin via the RGD fragment and inducing tumor cell apoptosis via the neovascular endothelium, which has been demonstrated that they can directly target tumor endothelial cells as well as $\alpha_v\beta_3$ and $\alpha_v\beta_5$ integrin-positive tumor cells to be a promising anticancer agent with tumor-selective apoptotic activity.[29] In this study, by optimizing the amount of RGD-L-TRAIL on the surface of MMBs, in vitro and in vivo US/MR imaging experiments confirm the tumor targeting dual modal imaging due to the excellent acoustic scattering of micro-sized bubbles and the existence of SPIOs. After imaging, the nano-sized SPIOs with RGD-L-TRAIL can enter into the cancer cells by nanoparticle and RGD-mediated endocytosis to inhibit tumorigenesis. Therefore, RGD-L-TRAIL@MMBs delivery system could offer opportunities to be a combined single platform with excellent synergic effects of molecular targeting cancer imaging and therapy.

2. Results

2.1. Construction and Characterization of RGD-L-TRAIL@MMBs

The construction of RGD-L-TRAIL@MMBs is illustrated in **Figure 1**A. We first modified the polyvinyl alcohol (PVA) with carboxyl group to obtain the polymeric MBs. Since PVA and carboxyl-modified PVA indicate the superior biocompatibility,[30,31] the PVA-based MBs can be potentially used in in vivo application. The zeta potential of carboxyl group modified PVA microbubbles and unmodified PVA microbubbles were −38.87 ± 2.19 and −0.68 ± 1.6 mV, respectively. The high negative charges of carboxyl group on the MBs endow the MBs with good dispersion stability, which has been demonstrated in Figure S1 (Supporting Information). Importantly, this carboxyl group enabled the possibilities of microbubbles to chemically bind with aminopropyltriethoxysilane (APTS) modified γ-Fe$_2$O$_3$ SPIOs. Thus, the stable carboxylated MBs then chemically react with the amino group on the SPIOs modified with APTS, a reaction that was catalyzed by 1-ethyl-3-(3-dimethylaminopropyl)carbodiimide (EDC)·HCl and N-hydroxysulfosuccinimide (NHS) and generated SPIO-coated MMBs. Since a lot of remaining amino of ATPS/γ-Fe$_2$O$_3$ were loaded on the surface, using the same method, carboxyl groups of RGD-L-TRAIL were conjugated to residual amino groups on the MMBs surface to produce RGD-L-TRAIL modified magnetic microbubbles, which was defined as RGD-L-TRAIL@MMBs. The Fourier transform infrared spectroscopy (FT-IR) results of RGD-L-TRAIL, MMBs, and RGD-L-TRAIL@MMBs (Figure S2A, Supporting Information)

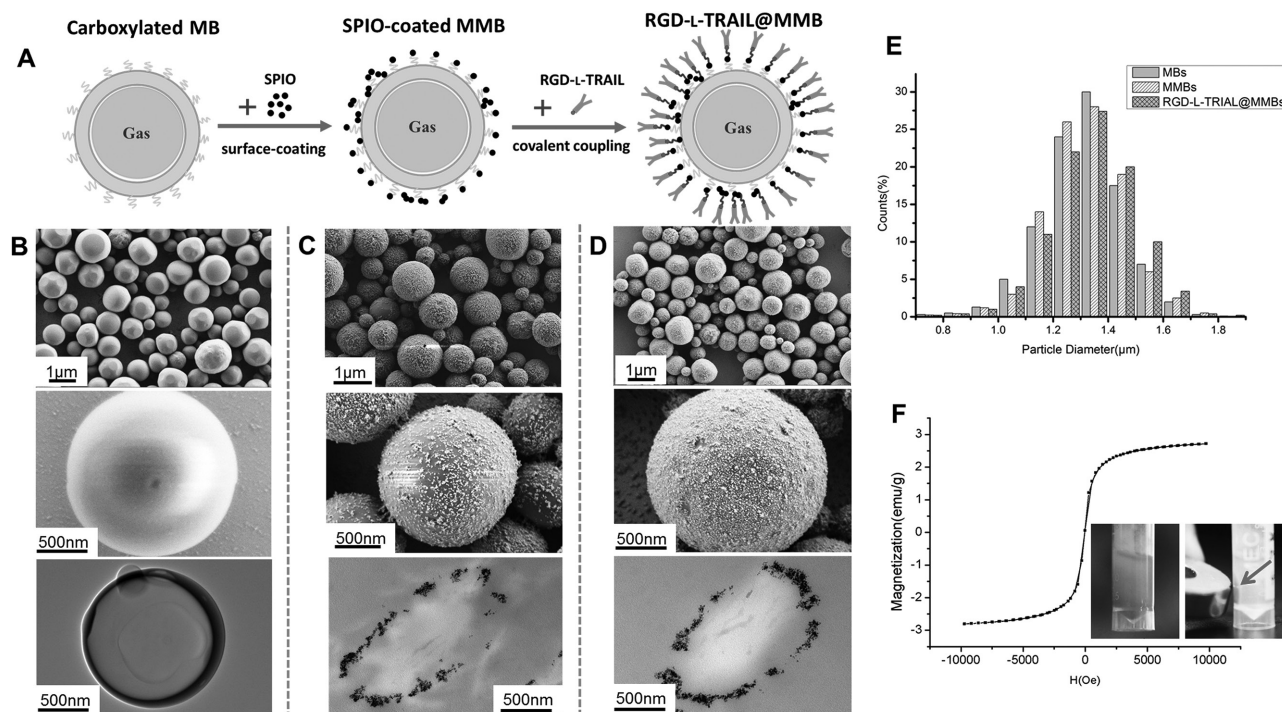**Figure 1.** A) Schematic diagram to show the construction of RGD-L-TRAIL@MMBs. SEM and TEM images of B) MBs, C) MMBs, and D) RGD-L-TRAIL@MMBs. E) Size distribution of MBs, MMBs, and RGD-L-TRAIL@MMBs. F) VSM curves of RGD-L-TRAIL@MMBs. Inset pictures of the movement of RGD-L-TRAIL@MMBs to external magnetic field (red arrows) have verified the RGD-L-TRAIL@MMBs to be endowed with magnet targeting characteristics.

www.MaterialsViews.com

ADVANCED
FUNCTIONAL
MATERIALS
www.afm-journal.de

FULL PAPER

indicated the chemical conjugation between RGD-L-TRAIL and MMBs. FT-IR of RGD-L-TRAIL, magnetic iron oxide nanoparticles (MNPs), and RGD-L-TRAIL@MNPs in Figure S2B (Supporting Information) further demonstrated the specific chemical attachment between RGD-L-TRAIL and MNPs.

Scanning electron microscopy (SEM) and transmission electron microscopy (TEM) images and microbubble size distribution of unmodified MBs, MMBs, and RGD-L-TRAIL@MMBs (with SPIO and protein contents of 2.10×10^{-7} μg per MMB and 2.30×10^{-6} μg per MMB, respectively) are shown in Figure 1B–E. The mean diameter of RGD-L-TRAIL@MMBs was 1.37 μm. The assembly of SPIO and RGD-L-TRAIL on the MB surface had no obvious effect on microbubble size (Figure 1E). Vibrating sample magnetometer (VSM) result shown in Figure 1F demonstrated that RGD-L-TRAIL@MMBs exhibited good superparamagnetic feature with a saturation magnetization value of 2.10 emu g^{-1}. The inset pictures in Figure 1F showed that the RGD-L-TRAIL@MMBs could be navigated by external magnetic field.

In order to further verify the layer-by-layer structural morphology, TEM images of MMBs and RGD-L-TRAIL@MMBs with enlarged surface structure have been shown in **Figure 2**, which clearly indicated RGD-L-TRAIL molecules were localized on the surface of SPIOs.

2.2. SPIO and RGD-L-TRAIL-Coupling Amount of MMBs

Since the MB shell structure is closely associated with its acoustic properties, the conjugation of SPIO and RGD-L-TRAIL protein on the MB surface was predicted to affect the structure and final US and MRI dual imaging. In preliminary experiment, in order to obtain the optimal US/MRI dual modality imaging, the optimal amount of SPIOs was detailed to study.
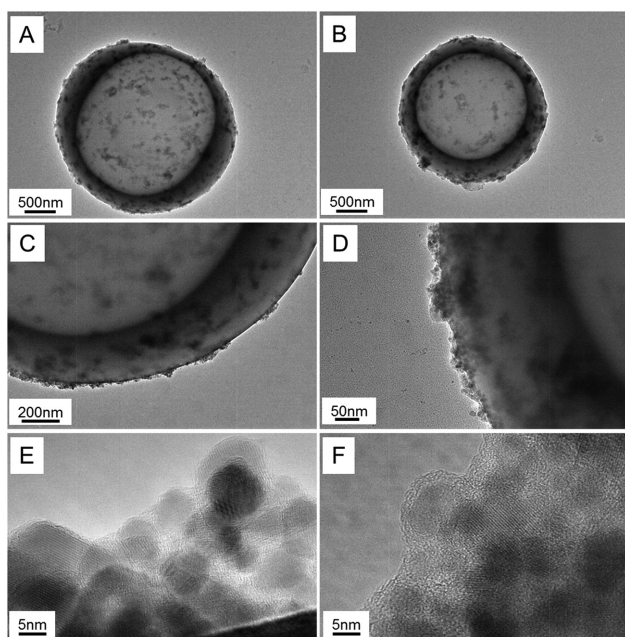

Figure 2. TEM images of A,C,E) MMB and B,D,F) RGD-L-TRAIL@MMB at different magnifications.

The results show that the US/MRI imaging was enhanced as a function of the amount of SPIO that was conjugated. However, the dispersion stability was concomitantly reduced. Based on these findings,[28] the 2.10×10^{-7} μg SPIO per MMB was used for further protein assembly.

RGD-L-TRAIL could be covalently conjugated on the MMBs using the reaction between amino groups of SPIO and carboxyl groups of RGD-L-TRAIL. The RGD-L-TRAIL molecules themselves can play two roles: targeting tumor vasculature and killing tumor cells due to the activity of RGD and TRAIL molecules, respectively. In theory, targeting sensitivity and tumor cell inhibition efficiency are proportional to the concentration of RGD-L-TRAIL on the surface of MMBs. Optical microscope images of RGD-L-TRAIL@MMBs before and after dyeing with the Coomassie Brilliant Blue G-250 were shown in **Figure 3**A,B. Different amounts of RGD-L-TRAIL were determined with the Coomassie Brilliant Blue G-250 assay shown in Figure 3C. Protein-conjugated MMBs form complexes with G-250, and the resultant color change can be quantitatively measured by ultraviolet–visible spectrophotometer. As the amount of added protein was increased, there was a concomitant increase in the amount of protein conjugated to MMBs. The maximum coupling amount of protein on the MMBs (sample #6) shown in Figure 3C indicated the 85.7% attached efficiency with amounts of the RGD-L-TRAIL of 642.60 μg mL^{-1}. However, Figure S3 (Supporting Information) showed that the dispersion stability of the MMBs decreased with the amount of protein added. Because molecular imaging probes used for medical purposes need to enter systemic circulation through blood vessels, there are strict requirements for dispersion stability. Hence, a balance between sensitivity and stability must be achieved. The sample #3 with protein contents of 229.50 μg mL^{-1} (61.0% attached efficiency) or 2.30×10^{-6} μg protein concentrations per MMB was chosen to be the optimal structure.

2.3. In Vitro US/MRI Imaging

In vitro US imaging was carried out using RGD-L-TRAIL@MMBs at a concentration of 1×10^8 MMBs mL^{-1}. Images were recorded every 20 s, and the average grayscale values in corresponding region of interests (ROIs) were used to plot average grayscale-time curves for each sample (**Figure 4**A,B). Upon RGD-L-TRAIL@MMBs injection, the brightness of images of simulated blood vessels in the phantom immediately increased. Over time, some MMBs began to rupture and image brightness gradually decreased. It is concluded that RGD-L-TRAIL@MMBs enhanced US imaging for ≈5 min in the in vitro experiment.

Furthermore, in vitro MRI was carried out using RGD-L-TRAIL@MMBs. The T$_2$-weighted images of RGD-L-TRAIL@MMBs with different volume fraction were shown in Figure 4C. The decreased T$_2$ signal value demonstrated the RGD-L-TRAIL@MMBs remained its suitability as a contrast agent for T$_2$ enhancement of MRI. R_2 values were calculated based on T$_2$ values based on different volume fraction of RGD-L-TRAIL@MMBs. Results in Figure 4D indicated that the R_2 values was linearly related to the volume fraction of RGD-L-TRAIL@MMBs ($r^2 = 0.99235$).
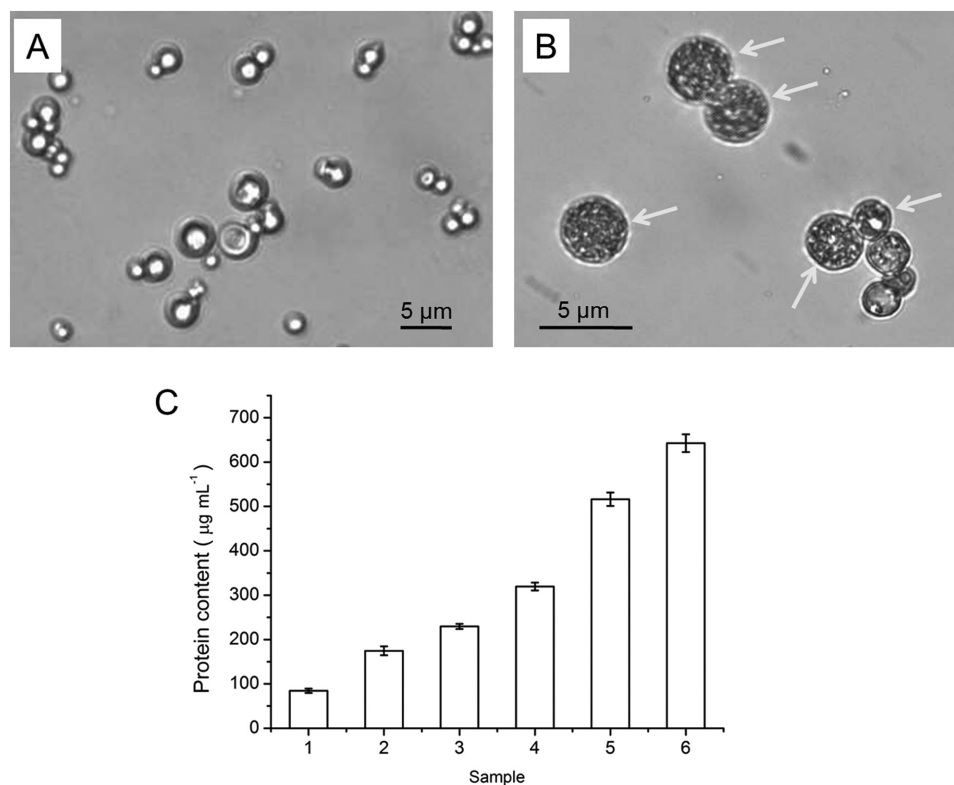
ADVANCED
FUNCTIONAL
MATERIALS
www.afm-journal.de

Materials Views
www.MaterialsViews.com

FULL PAPER

Figure 3. Optical microscopy images of RGD-L-TRAIL@MMBs A) before and B) after dyeing with the Coomassie Brilliant Blue G-250. C) Sample Nos. 1–6 are the RGD-L-TRAIL@MMBs with protein contents of 84.4, 174.5, 229.5, 319.5, 516.2, and 642.6 µg mL^{-1}, respectively.

2.4. Apoptosis of COLO-205 Colon Cancer Cells Induced by RGD-L-TRAIL@MMBs

The in vitro tumor cell targeting and apoptosis-inducing capabilities of RGD-L-TRAIL@MMBs were confirmed using COLO-205 colon cancer cells treated with MMBs, RGD-L-TRAIL, or RGD-L-TRAIL@MMBs, respectively. **Figure 5**A–C of the statistical apoptosis flow cytometry results in MMBs, RGD-L-TRAIL@MMBs (400 ng protein mL^{-1}), and RGD-L-TRAIL (400 ng protein mL^{-1}) groups were 3.6%, 86.7%, and 94.3%, respectively, which clearly demonstrated that apoptosis from RGD-L-TRAIL@MMBs group is comparable to the RGD-L-TRAIL group. This evidence further indicated that after conjugation of RGD-L-TRAIL on the structure of MMBs, the biological activity of RGD-L-TRAIL has been maintained. Further, the apoptosis rate of tumor cell shown in Figure 5D was in a dose-dependent manner by RGD-L-TRAIL@MMB group.

2.5. In Vivo US Imaging

To evaluate the in vivo US targeting imaging effect, colon tumor bearing nude mice were injected intratumorally or via the caudal vein with MMBs or RGD-L-TRAIL@MMBs and then imaged by US. **Figure 6**A,C showed that both intratumorally and intravenous injection of RGD-L-TRAIL@MMBs can make the tumor US images brighter than MMBs injection group. For both RGD-L-TRAIL@MMBs and MMBs group, the US enhancement of intratumoral injection was

stronger than intravenous injection. ROIs at different time points were selected from US images of tumors and used to calculate average grayscale values and generate grayscale-time curves for intravenous and intratumoral injection. Figure 6D indicated that grayscale values increased within 2 min of intratumoral injection of MMBs or RGD-L-TRAIL@MMBs. However, for RGD-L-TRAIL@MMBs group, the brightness of US imaging can be remained for about 10 min. For MMBs group, the enhancement of imaging was decreased after 2 min. The intravenous injection results shown in Figure 6B demonstrated the similar changes after 6 min injection observation. Also, the RGD-L-TRAIL@MMBs group confirmed the better tumor US imaging effect. The reason of delayed targeting US imaging resulting from the intravenous injection may be that through caudal vein microbubbles can only reach the tumor site by blood circulation, which needs longer time to accumulate in tumor site to enhance the imaging. Although there is difference between intratumoral and intravenous injection, the RGD-L-TRAIL@MMBs maintaining the US enhancement for more than 10 min exhibited the good targeting efficiency of RGD-L-TRAIL@MMBs to tumor neovasculature.

2.6. In Vivo MRI

Similarly, the in vivo MR targeting imaging enhancement was verified. Nude mice were injected via the caudal vein (Figure 6E) or intratumorally (Figure 6F) with MMBs or RGD-L-TRAIL@MMBs and imaged by MRI. MMBs and RGD-L-TRAIL@MMBs

www.MaterialsViews.com

ADVANCED
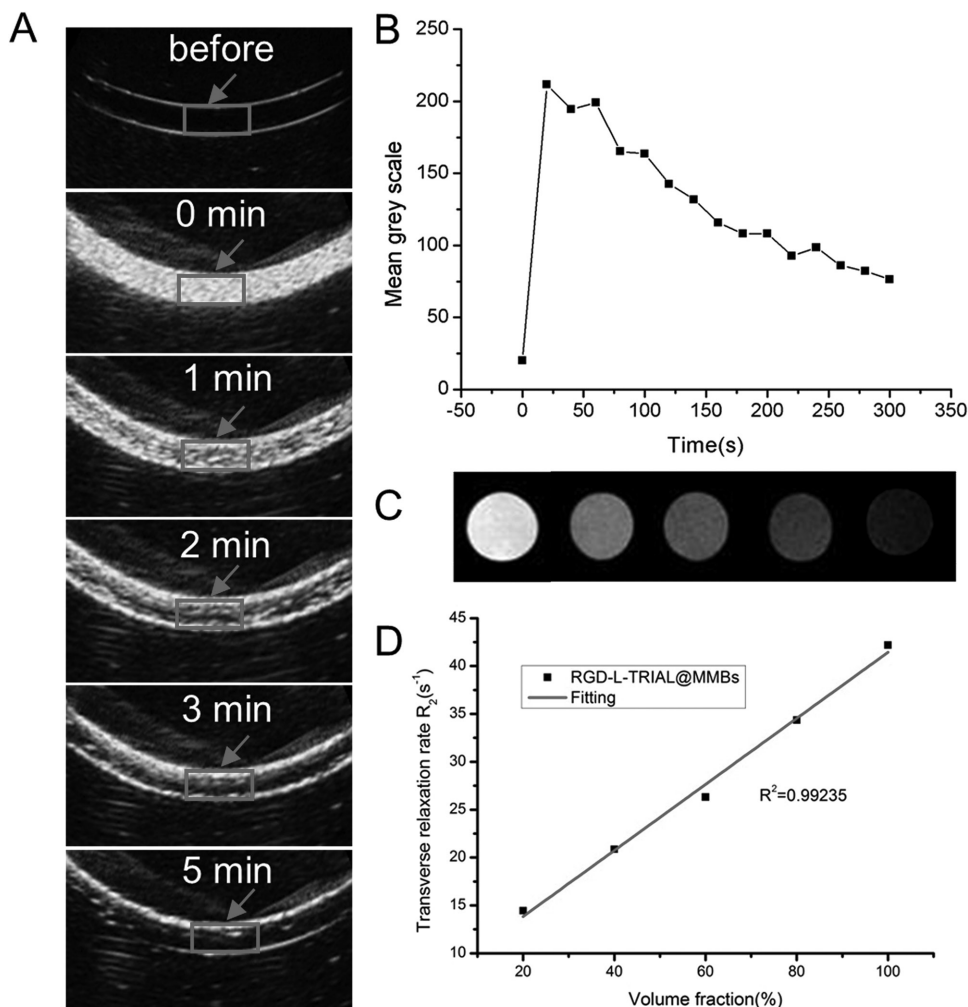FUNCTIONAL
MATERIALS
www.afm-journal.de

FULL PAPER

Figure 4. A) In vitro ultrasound images over time. B) The mean grayscale-time curve of the RGD-L-TRAIL@MMBs of US imaging enhancement. C) In vitro MRI images of the RGD-L-TRAIL@MMBs. D) Relationship between R_2 and volume fraction of RGD-L-TRAIL@MMBs.

both showed a greater enhancement on the T_2 signal of MR images when injected directly into the tumor as compared to through the caudal vein. This was predictable since intratumor fixed-point delivery avoids the loss of probe in the circulation. In addition, regardless of the mode of injection, changes in T_2 signal strength were more pronounced by injection of RGD-L-TRAIL@MMBs as compared to MMBs. This can be explained by the targeting of RGD-L-TRAIL@MMBs and consequent enrichment in tumors. After MBs ruptured, the released RGD-L-TRAIL and SPIO can be retained at tumor sites to be imaged by MRI. Without RGD-L-TRAIL targeting ligand, MMBs were easily removed with the blood and cannot be imaged by MRI for longer time. These MRI results are consistent with those obtained by US imaging and confirmed that RGD-L-TRAIL@MMBs are also an effective MRI contrast agent.

2.7. Distribution of Magnetic Nanoparticles and RGD-L-TRAIL in Tumors

The distribution of RGD-L-TRAIL@MMBs in tumor tissue was assessed by staining tumor tissue sections with Prussian blue to localize SPIO and by immunohistochemical (IHC) detection of TRAIL expression 24 h after caudal vein (**Figure 7**A1,B1) or intratumoral (Figure 7C1, D1) injection of RGD-L-TRAIL@MMBs or MMBs. Particles in the images that were stained blue were SPIO or MMBs carrying SPIO. Figure 7A2,B2,C2,D2 showed corresponding IHC staining results, and the areas in the images that were stained dark or pale brown represented positive areas for RGD-L-TRAIL.

As expected, Prussian blue staining and TRAIL immunoreactivity were higher in tumor tissue sections from animals' intratumorally injection with RGD-L-TRAIL@MMBs as compared to those injected via the tail vein. There was negligible immunoreactivity in sections from animals injected with MMBs by either route of administration, although Prussian blue staining was observed in tumors that were directly injected with MMB. Moreover, RGD-L-TRAIL@MMBs have the targeting property to specific accumulation in tumors through blood circulation and to release SPIO and RGD-L-TRAIL, which makes the tissue section stained as blue and brown (Figure 7A1, A2), respectively. This result also indirectly proved the effective coupling of RGD-L-TRAIL and SPIO in the structure of microbubbles.
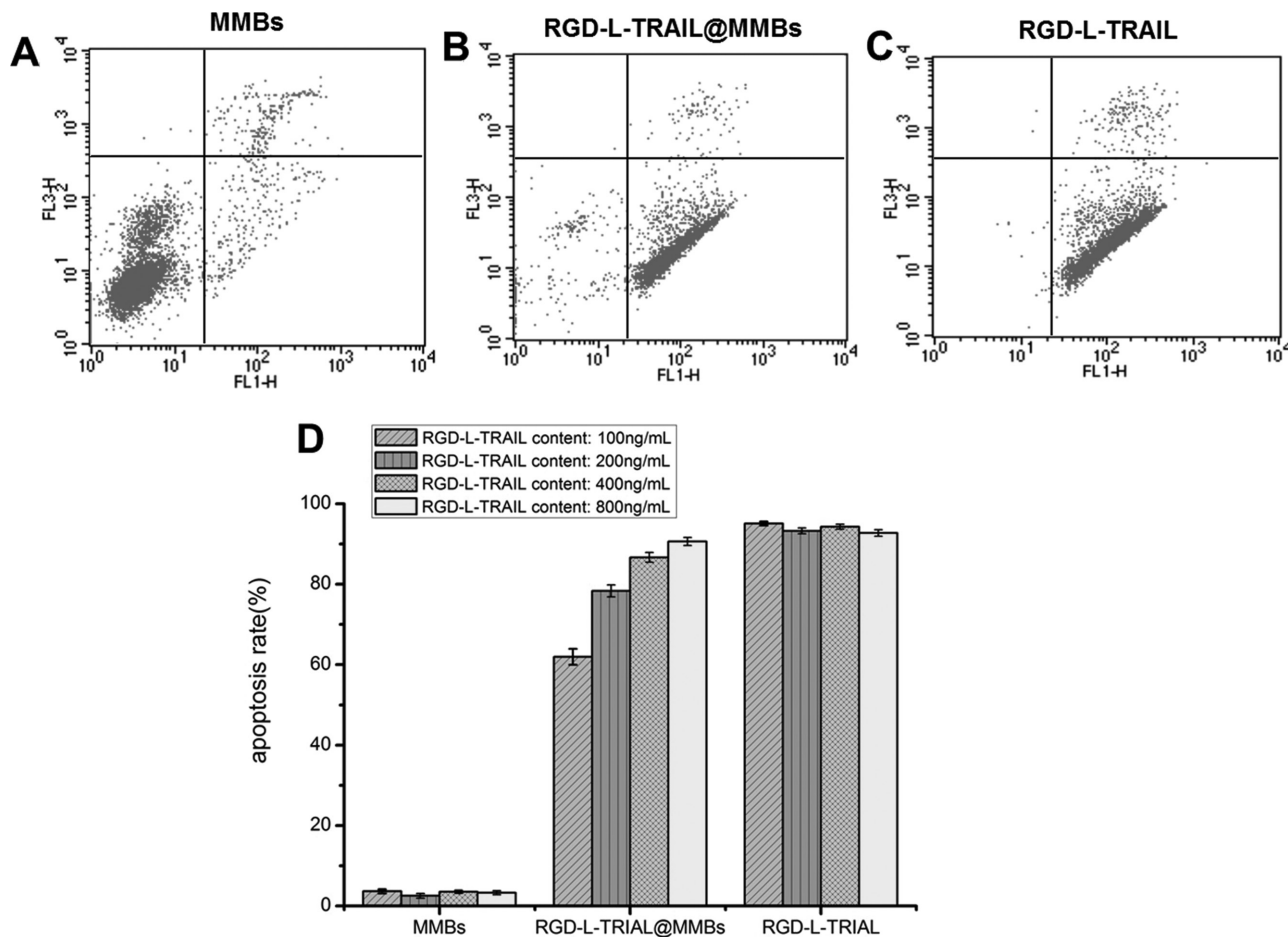
FULL PAPER

Figure 5. In vitro COLO-205 cell apoptosis induction treated with A) MMBs, B) RGD-L-TRAIL@MMBs, and C) RGD-L-TRAIL (400 ng protein mL^{-1}). D) Apoptosis rates of MMBs, RGD-L-TRAIL@MMBs, and RGD-L-TRAIL with different doses.

Furthermore, comparison between Figure 7C1,D1 showed that the staining was mainly localized in peripheral areas of tumor tissues and at injection sites in MMB-injected tissue, in contrast with the interstitial areas that were labeled in the case of RGD-L-TRAIL@MMB injection, confirming the tumor targeting of RGD-L-TRAIL@MMBs.

2.8. Therapeutic Effects of RGD-L-TRAIL@MMBs

To evaluate the in vivo therapeutic effects of RGD-L-TRAIL@ MMBs on colon cancer, the tumor therapeutic efficacy was tested. Average tumor size was determined and used to generate tumor size-time curves. **Figure 8**A clearly demonstrated that injection of RGD-L-TRAIL or RGD-L-TRAIL@MMBs could inhibit the growth of colon cancer xenografts. Whereas MMB-treated tumors did not differ significantly from the control group. In addition, there is no noticeable mortality and body weight discrepancies (Figure 8B) among control, MMBs, RGD-L-TRAIL, or RGD-L-TRAIL@MMBs, indicating a well-tolerated dose level and the biosafety of the RGD-L-TRAIL@MMBs. During the 20 d observation, all tumor-bearing mice survived.

Tumor cell apoptosis in each group was evaluated with the TUNEL assay (Figure 8C). The number of apoptotic cells

was higher in mice injected with RGD-L-TRAIL or RGD-L-TRAIL @MMBs, with apoptosis indices of (41.6 ± 0.06%) and (35.8 ± 0.04%), respectively. In contrast, the rate of apoptosis in animals injected with MMBs (3.0 ± 0.01%) was similar to that in controls (2.3 ± 0.01%). These results are in agreement with the enhanced growth inhibition observed in mice treated with RGD-L-TRAIL or RGD-L-TRAIL@MMBs as compared to the other groups.

3. Discussion

In order to maximize the diagnostic accuracy and therapeutic validity for cancer, it is essential to design a delivery system which maximizes its payloads to a cancerous lesion in spatial-, temporal-, and dosage-controlled fashions. However, the complex microenvironment inside the human body makes it hard to design targeted carriers with combination of high diagnostic sensitivity, specificity, and therapeutic efficacy.

In this work, we demonstrate a multi-gradient continuous targeting strategy based on RGD-L-TRAIL -labeled magnetic microbubbles for cancer therapy shown in **Figure 9**. The SPIOs on the shell of microbubbles have endowed the simultaneous magnetic resonance imaging and magnetic targeting to direct
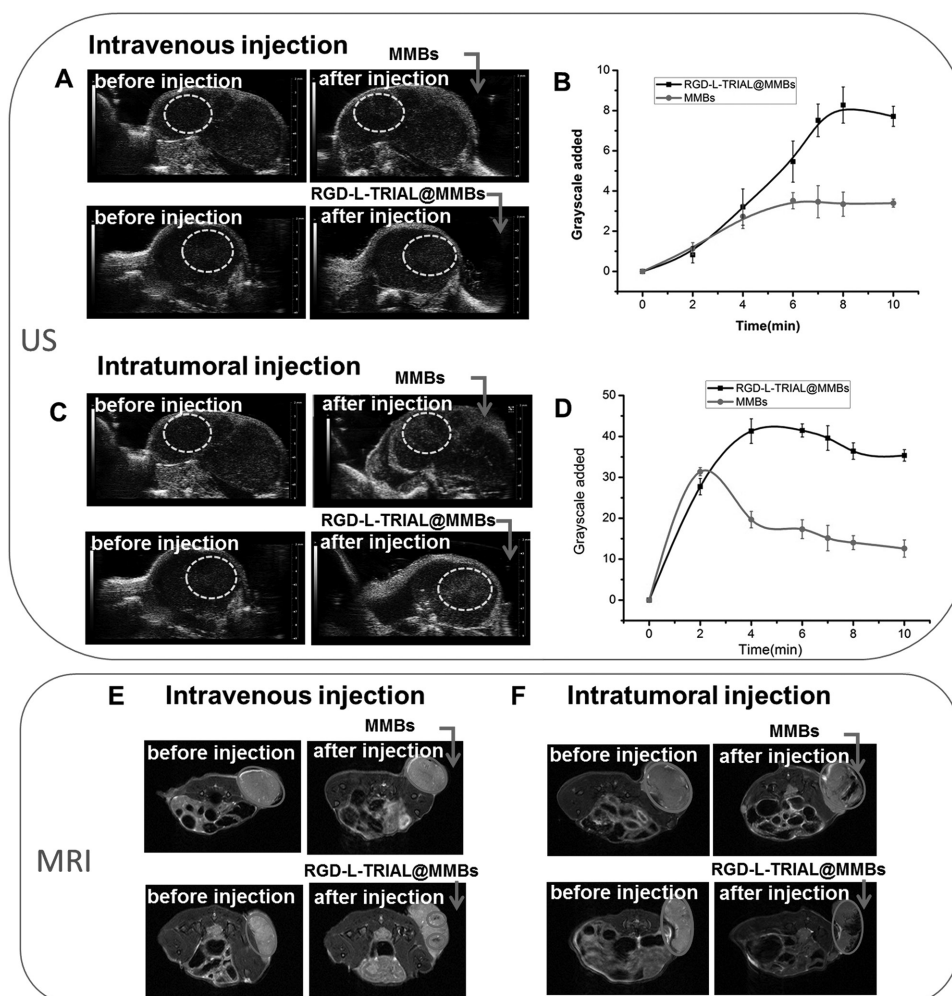
www.MaterialsViews.com

ADVANCED
FUNCTIONAL
MATERIALS
www.afm-journal.de

FULL PAPER

Figure 6. In vivo US and MR imaging results. A) Contrast-enhanced US images before and after intravenous injection of the MMBs and RGD-L-TRAIL@MMBs. B) Grayscale added-time curve of the US images after intravenous injection. C) Contrast-enhanced US images before and after intratumoral injection of the MMBs and RGD-L-TRAIL@MMBs. D) Grayscale added-time curve of the US images after intratumoral injection. T_2 MR images before and after (4 h) the E) intravenous injection and F) intratumoral injection of the MMBs and RGD-L-TRAIL@MMBs.

microbubbles and RGD-L-TRAIL protein to tumor sites. Meanwhile, the SPIOs on the shell of microbubbles were further decorated with RGD-L-TRAIL protein to enhance the targeting efficiency of tumor angiogenesis. Additionally, after the disruption of microbubbles, the RGD-L-TRAIL would be efficiently internalized by cancer cells via integrin $\alpha_v\beta_3$-receptor-mediated endocytosis mechanism to enhance the efficacy of cancer treatment.[29] Thus, this smart designed RGD-L-TRAIL@MMBs system has a complex but elaborate multilayer structure: gas in the core for US imaging, SPIO on the shell for MRI imaging and magnetic targeting control, and RGD-L-TRAIL ligand for enhanced combination of tumor-targeted delivery of TRAIL. First, RGD-L-TRAIL protein on the MMBs surface enables the microbubbles to actively target to the tumor angiogenesis. The micro-scaled bubbles size around the tumor is beneficial for real-time US imaging and MRI to clearly delineate the tumor margin shown in Figure 6. Second, after US imaging, with the rupture of microbubbles in situ around the tumor, nanoscaled SPIOs with RGD-L-TRAIL molecules can go through the blood

vessel and enter into the tumor tissue due to both the tumor passive enhanced permeability and retention effect and RGD-L-TRAIL ligand induced integrin $\alpha_v\beta_3$-receptor-mediated endocytosis, which has been demonstrated in Figure 7. At this stage, tumor tissue can also be imaged by MRI. During this process, with the accumulation of RGD-L-TRAIL and SPIOs in the tumor tissue and cells, the tumor apoptosis shown in Figure 8 induced by TRAIL molecules can also be observed. Moreover, since the SPIOs were still retained in the tumor tissue, MRI can be used to assess tumor progression and treatment outcome with no other contrast agents injected again.

Further improving the sensitivity and specificity of molecular imaging modalities will be essential for cancer diagnosis and staging in order to ultimately be able to detect even the smallest malignant lesions, which is largely dependent on molecular imaging probe design. Further advances in molecular imaging probe design, such as attaching other kind of contrast agent (e.g., SPIO), or chemotherapeutic drugs, as well as increasing probe accumulation in the tumor, will
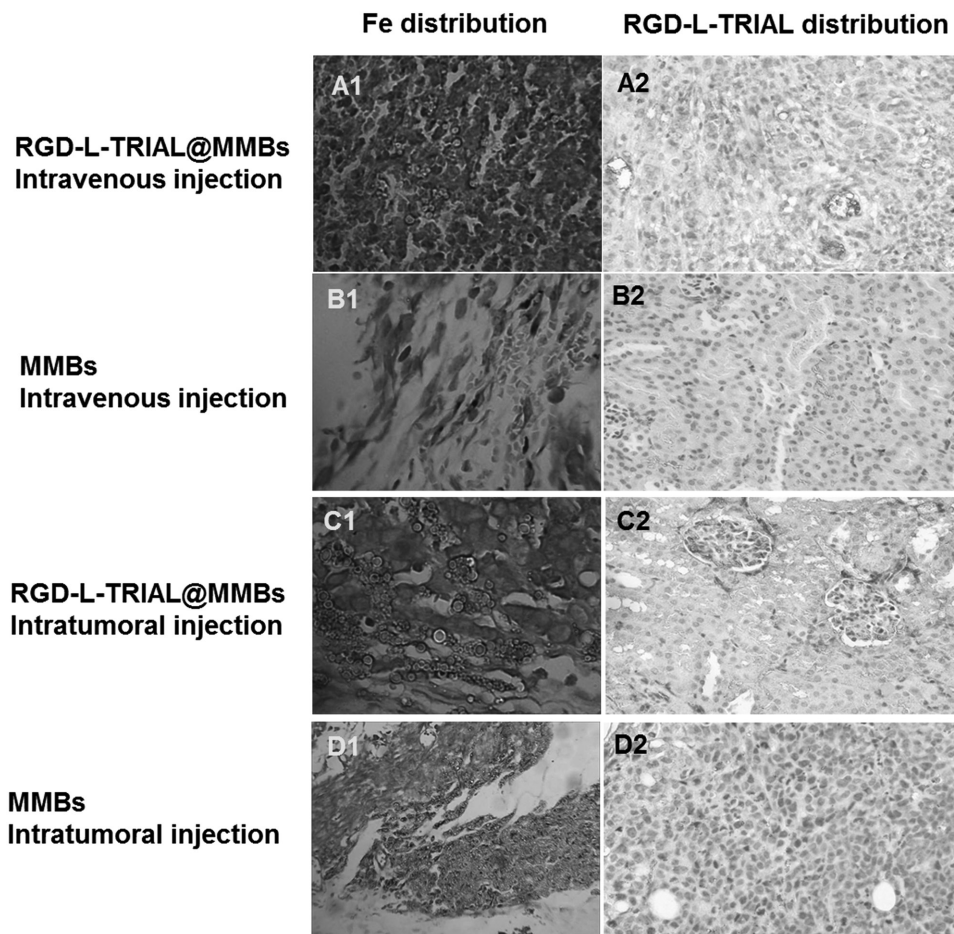
ADVANCED
FUNCTIONAL
MATERIALS
www.afm-journal.de

FULL PAPER

Materials
Views
www.MaterialsViews.com

Figure 7. Distribution of A1–D1) Fe and A2–D2) RGD-L-TRAIL in tumors after the injection of the MMBs and RGD-L-TRAIL@MMBs.

be necessary to increase sensitivity in the future. Although probes with varying target sensitivity/specificity are currently in use or being investigated,[32–37] some logistical aspects need to be taken into consideration that the development of molecular imaging probes with a broader targeting design to enhance the delivery performance at the target site (spatial control) and at the right time (temporal control). In this study, although the RGD-L-TRAIL itself has been reported to indicate the antitumor efficacy in vitro and in vivo by targeted delivery to tumors, unforeseen immunologic effects, or hepatic dysfunction, as well as fast clearance are still the main limitation for future clinical applications.[38] The ability to monitor treatment will allow physicians to prevent overtreatment or under-treatment. The theranostic RGD-L-TRAIL formulations may provide excellent diagnosis modality for imaging guided and monitored RGD-L-TRAIL tumor targeting and therapy. Thus, the fabrication of RGD-L-TRAIL@MMBs system based on the aforementioned multi-gradient continuous targeting strategy can enable tumor treatment monitoring with a one-time administration of delivery system to potentially facilitate the accurate dual US/MRI guidance and released TRAIL molecules to induce cell apoptosis. It is promising considerable synergistic benefits for potential future clinical utility.

4. Conclusion

With the development of the novel molecular imaging techniques, it is possible to design targeted multimodal imaging contrast agents carrying therapeutic payloads for one-time administration paradigm of cancer theranostics. We demonstrated that RGD-L-TRAIL@MMBs can be used to enhance US and MRI of tumors and that they are specifically taken up by tumors and induce apoptosis of tumor cells. These findings indicate that this probe is suitable as a multi-modal and multi-functional multi-gradient targeting drug delivery system for effective tumor diagnosis and treatment. Such engineerable RGD-L-TRAIL@MMBs structures exhibit significant advantages including increased contrast sensitivity, binding avidity, and targeting specificity.

5. Experimental Section

Materials: The APTS-coated SPIO γ-Fe$_2$O$_3$ (ATPS/γ-Fe$_2$O$_3$) NPs (mean diameter: 10 nm, mean hydrodynamic diameter: 64.9 nm) were provided by the Jiangsu Key Laboratory for Biomaterials and Devices (China).[39] PVA (molecular weight (M_w): 31 000) was obtained from Sigma-Aldrich (USA) and poly-L-lactic acid (PLLA) (M_w: 30 000) from Jinan Jian Bao Kai Yuan Biological Material Company (China). Sodium periodate (NaIO$_4$)

www.MaterialsViews.com

ADVANCED
FUNCTIONAL
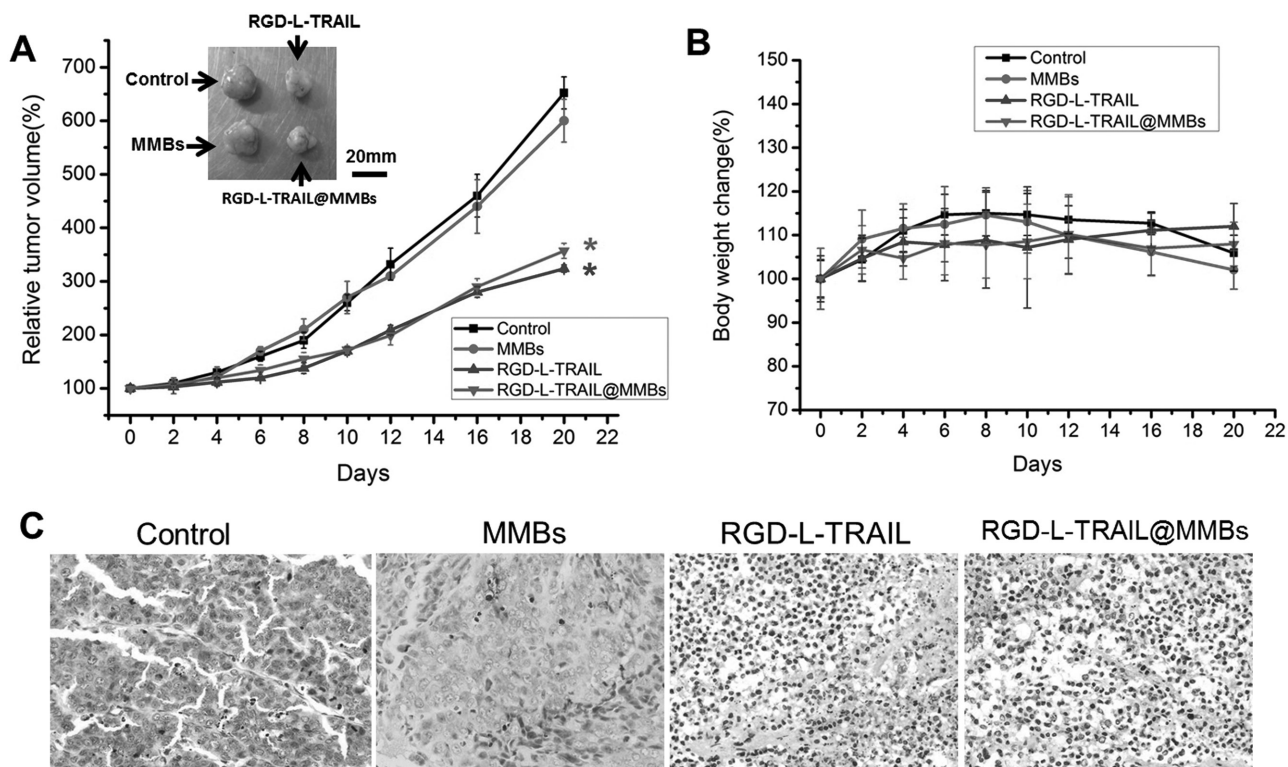MATERIALS
www.afm-journal.de

FULL PAPER

Figure 8. Antitumor effect of RGD-L-TRAIL@MMBs in colon cancer subcutaneous model. A) Analysis of tumor growth (relative to day 0) as a function of time for the untreated control tumors ($n = 4$), tumor treatments with MMBs ($n = 6$), with RGD-L-TRAIL ($n = 6$) and with RGD-L-TRAIL@MMBs ($n = 6$). The results were expressed as the mean ± SD for each group. *$p < 0.05$ compared with the control group. B) Body weight changes of tumor-bearing mice after treated with control, MMBs, RGD-L-TRAIL, or RGD-L-TRAIL@MMBs. C) Representative microscopy images of TUNEL assays for apoptotic cell death (magnification 400×).

was purchased from Guangdong Product Engineering Technology Research and Development Center (China). Sodium chlorite ($NaClO_2$) was purchased from Shanghai Jingchun Reagent Company (China). EDC and NHS sodium salt were procured from Shanghai Medpep Company (China). 2-(N-morpholino)ethanesulfonic (MES) acid was procured from Nanjing Shengxing Biological Technology Company (China), RGD-L-TRAIL protein, molecular weight of ≈21 000 Da, was provided by Nanjing University State Key Laboratory for Medical Biotechnology.[29]
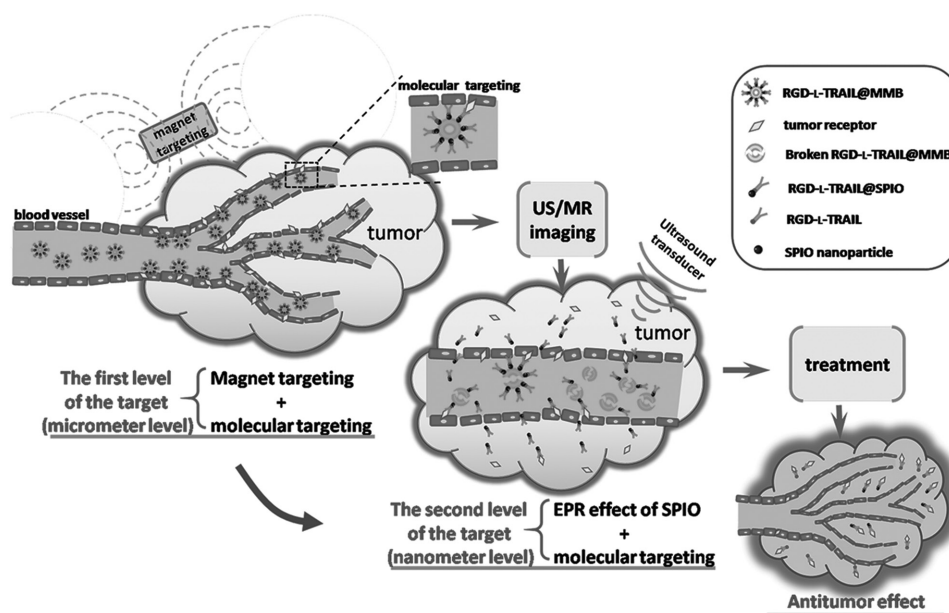

Figure 9. Schematic diagram showing multi-gradient targeting strategy of RGD-L-TRAIL@MMBs for the tumor diagnostics and therapy.
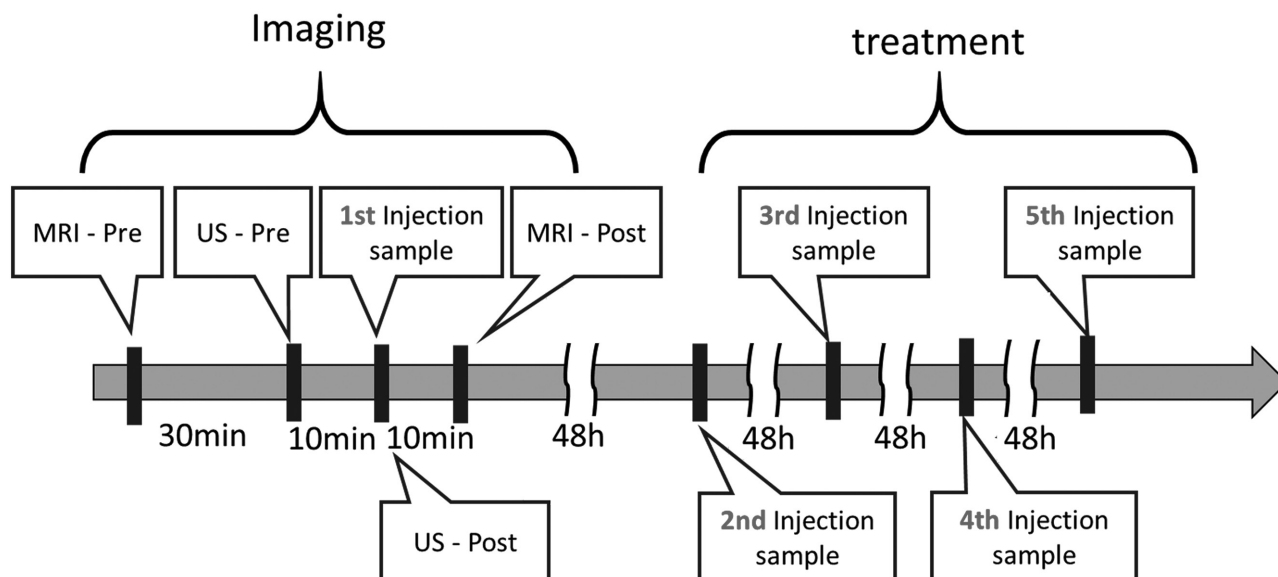
Figure 10. In vivo protocol diagram of time course of imaging and treatment.

The human colon cancer cell line COLO-205 was obtained from the Type Culture Collection of the Chinese Academy of Sciences (Shanghai, China). Span20, Tween80, N_2, and other reagents were analytical grade.

Fabrication of RGD-L-TRAIL@MMB: The purified ATPS/γ-Fe$_2$O$_3$ MMBs were formed via double emulsion/ solvent evaporation as previously described.[28] Then by using the amino bonds on the ATPS/γ-Fe$_2$O$_3$ surface, the RGD-L-TRAIL protein molecules were chemically conjugated with MMBs. Briefly, after washed three times by distilled water, MMBs samples were suspended in MES buffer (50 × 10^{-3} M, pH = 5.4). RGD-L-TRAIL was dissolved in MES buffer (50 × 10^{-3} M, pH = 5.4), the solution was activated by EDC (0.4 mg mL^{-1}) and NHS (0.6 mg mL^{-1}) at room temperature, then incubated with a certain amount of MMBs suspension at 4 °C. After 3 h, RGD-L-TRAIL@MMBs were collected using magnetic isolation method. The separation process was stopped until the supernatant solution cannot make the Coomassie Brilliant Blue G250 discolorate. Generally, five times washing was needed.

Characterization of RGD-L-TRAIL@MMB: The morphology of RGD-L-TRAIL@MMBs was examined using SEM (Ultra Plus, Carl Zeiss, Germany) and TEM (JEM- 2100, the Japanese JEOL company). The particle size distribution was examined using optical microscopy (BM1000, Jiang Nan Optical Company, China). Images were obtained at 400× magnification. Samples were taken from each of the three batches, and ten images were taken from each sample. The size distribution of RGD-L-TRAIL@MMBs was then obtained using purpose-written image analysis software in MatLab.[40] The number concentration of RGD-L-TRAIL@MMBs was measured with a hemocytometer. The Fe content of the APTS/γ-Fe$_2$O$_3$ NPs assembled onto the shells of the MBs was determined from the corresponding absorbance versus iron concentration (r^2 = 0.9999) calibration curve, which was determined using the 1,10-phenanthroline spectrophotometric method.[41] The ultraviolet–visible (UV–vis) spectrophotometer (UV-3600, Shimadzu, Japan) was employed to quantify the Fe concentration at the wavelength of 510 nm. The RGD-L-TRAIL protein content coupling on the MMB was evaluated with Brandford method by automatic microplate reader (Thermo Labsystems 1500, USA). The magnetization properties of the RGD-L-TRAIL@MMB were characterized using a VSM (Model 7407, Lake Shore Cryotronics, Inc., USA), all the samples were tested in dry powder form.

In Vitro US Imaging: In vitro US imaging was performed using a laboratory-made agar power phantom, in which a cellulose tube pipeline was put in the phantom for sample loading. The test samples were imaged using a digital B-mode diagnostic ultrasonic instrument (Belson 3000A, Belson Imaging Technology Co., Ltd., China) with a 3.5 MHz

R60 convex array probe. A suspension of the RGD-L-TRAIL@MMB was injected into the pipeline of the phantom and was imaged by the US instrument. The concentrations of samples were 1 × 10^8 MBs mL^{-1}. Distilled and degassed water was used as the control sample. The mean grayscale values of the US images were measured by using the imaging analysis software Image J. When a ROI was selected, its mean grayscale value was calculated automatically. Three scanned segments (ROIs) were processed for each sample, and the average mean grayscale value was used.

In Vitro MRI: In vitro MRI was performed on a 7.0 T system (Micro-MRI, PharmaScan, Bruker, Germany). A suspension of the RGD-L-TRAIL@MMB with concentration of 1 × 10^8 MBs mL^{-1} was studied. The sample was diluted to different volume fractions from 100% to 20% by adding distilled water. To obtain the absolute T_2 relaxation times, a multi-slice, multi-echo T_2 map sequence was used. The scan parameters were as follows: TR of 3000 ms, TE of 12–192 ms in steps of 12 ms, field of view (FOV) of 60 × 60 mm, matrix size of 256 × 256, and slice thickness of 1 mm. The T_2 relaxation times were calculated using the post-processing software ParaVision 5.0. The transverse relaxation rate (R_2) as a function of MBs volume fraction was then calculated based on the measured T_2 data.

In Vitro COLO-205 Cell Apoptosis Induction Experiment: The human colon cancer cell COLO-205 was used to detect whether RGD-L-TRAIL@MMB keep the activity of inducing cell apoptosis. Three samples were selected: (1) MMBs, (2) RGD-L-TRAIL@MMBs, and (3) RGD-L-TRAIL; samples (1) and (2) have the same particle size and the number concentration of microbubbles; samples (2) and (3) have the same protein content. Three kinds of samples above were diluted with protein content concentration gradient of 100, 200, 400, and 800 ng mL^{-1}, inducing the COLO-205 cell, respectively, processing time is 2.5 h. Cell apoptosis was determined by using Annexin V- FITC and pyridine iodide (PI) double staining with flow cytometry instrument (FACSCalibur, BD companies in the United States). Determination of each sample was repeated three times.

Animal Model and Experimental Protocol: 30 female BALB/C nude mice, aged 4–6 weeks, were obtained from the Center of Laboratory Animal Sciences of Nanjing Medical University (China). All animal procedures were performed in compliance with the animal experimentation guidelines of the Animal Research Ethics Board of Southeast University. ≈10^6–10^7 COLO-205 cells were inoculated subcutaneously into the right flanks of the nude mice, and tumors were allowed to grow for 10–14 d prior to the experiment. As exemplified by **Figure 10**, the detailed imaging and therapeutic study protocol of in

www.MaterialsViews.com

ADVANCED
FUNCTIONAL
MATERIALS
www.afm-journal.de

FULL PAPER

vivo has been designed. RGD- L-TRAIL-containing MMBs were injected into tumor-bearing mice. The targeting and accumulation of released SPIOs in tumor tissue were visualized and quantified using US/MR dual modal imaging. In parallel, the therapeutic effect of RGD-L-TRAIL was evaluated. Such theranostic strategies are considered to be useful for efficiently and safely treating tumor.

In Vivo Tumor US Imaging: Eight nude mice were selected and randomized into two groups. One group was injected with MMBs. The second group was injected with the RGD-L-TRAIL@ MMBs. The concentrations, i.e., number of MBs per volume, MB sizes, and SPIO content ([MB] = 1×10^8 MBs mL^{-1}, average diameter = 1.37 μm, [SPIO] = 2.1×10^{-7} μg per MMB) were comparable between samples with the MMBs and RGD-L-TRAIL@ MMBs. All mice were kept anesthetized with 2% isoflurane in oxygen-enriched air using a facemask during the entire imaging process. In vivo US imaging was performed using a small animal US imaging system (Visualsonics Vevo2100, Canada). The tumors were scanned 3D prior to injection to confirm a clear background signal. The US tumor images were obtained in real time after 200 μL of the MMBs or RGD-L-TRAIL@ MMBs dispersion had been injected intratumorally or intravenously. The imaging settings for the US system were a center frequency (*f*) of 30 MHz and a gain of 20 dB. The mean grayscale values in the ROIs of the tumors were analyzed and normalized to the grayscale values before injection of the samples. US imaging observation lasted 10 min.

In Vivo Tumor MRI: Before and after each US imaging procedure, MR imaging was accomplished through a 7.0 T scanner (Micro-MRI, PharmaScan, Brukers, Germany) equipped with a 3.8 cm circular coil, a 2D T_2 fast low-angle shot sequence with respiratory gating control was employed. The parameters were TR/TE = 100 ms/8 ms, flip angle = 350°, FOV = 10×10 mm, slice thickness = 2 mm, number of excitations = 2, in-plane resolution = 0.78×0.78 mm^2, and temporal resolution = 21 s. To evaluate the contrast, the signal intensities in the ROIs covering the tumors were measured before and after the injection of the MBs by using the imaging analysis software Image J (NIH, USA).

Treatment Regimen: The remaining 22 mice were divided into four groups: group I (control, *n* = 4); group II (RGD-L-TRAIL, *n* = 6), group III (MMBs, *n* = 6), and group IV (RGD-L-TRAIL@ MMBs, *n* = 6). Injection was performed through caudal vein of nude mice according to separated groups above, once every 2 d, five times consecutively; the dosage is 200 μL per mouse. Group III and group IV had the same MBs concentration and SPIO contents, while group II and group IV had the same protein content.

Histopathological Analysis: After each in vivo US/MR imaging experiment, the mouse was euthanized by a lethal dose of pentobarbital. All of the tumors were harvested and fixed in 10% neutral buffered formalin, processed and paraffin embedded for the histopathological analysis for the distribution of iron nanoparticles and RGD-L-TRAIL. The Prussian blue stain was used to detect the iron distribution in tumor tissue. The specific steps are as follows: Taking nude mice tumor tissue section, washing with PBS repeatedly, and then adding the compound of 10% potassium ferrocyanide and 2% hydrochloric acid, incubating for 30 min at 37 °C, PBS washing, staining with neutral red dye, finally, the stained blue tumor tissue was observed under the microscopy. To determine RGD-L-TRAIL distribution in tumor, tumor tissue sections were stained with antibodies against TRAIL which marks the RGD-L-TRAIL.

For apoptosis of tumor cells, tumors were harvested from 22 mice after treatment at day 20. All harvested tumors were fixed in 10% neutral buffered formalin, routinely processed and paraffin embedded. Apoptosis was evaluated on these tissue sections using TdT-mediated dUTP nick end labeling (TUNEL assay) method. Apoptosis expression was detected with a microscope. The apoptotic index (AI) expressed as the ratio of positively stained tumor cells to all cells was determined from at least five random selected high power (400× magnification) fields.

Measurement of Tumor Volume: The size of nude mice tumor in each group was measured with Vernier calipers and was observed for 20 d and then once every 2 d. The tumor volume was calculated by following Equation (1)

$$\text{Tumor volume} = \frac{(\text{Tumor length}) \times (\text{Tumor width})^2}{2} \quad (1)$$

Relative tumor volumes were calculated by following Equation (2)

$$\text{Relative tumor volumes} = \frac{V_t}{V_c} \quad (2)$$

where V_c was the mean volume of the control group and V_t was the mean tumor volume of the treated groups.

Statistical Analysis: Results were reported as mean values with standard deviation (SD). Statistical differences for multiple groups were determined using a one-way ANOVA and individual groups were compared using Student's *t*-test. Probabilities of $p < 0.05$ were considered as significant difference.

Supporting Information

Supporting Information is available from the Wiley Online Library or from the author.

Acknowledgements

[1]   S. M. Janib, A. S. Moses, J. A. MacKay, *Adv. Drug Delivery Rev.* **2010**, *62*, 1052.

[2]   T. Hussain, Q. T. Nguyen, *Adv. Drug Delivery Rev.* **2014**, *66*, 90.

[3]   C. Wang, L. Cheng, Y. M. Liu, X. J. Wang, X. X. Ma, Z. Y. Deng, Y. G. Li, Z. Liu, *Adv. Funct. Mater.* **2013**, *23*, 3077.

[4]   B. Jang, H. Kwon, P. Katila, S. J. Lee, H. Lee, *Adv. Drug Delivery Rev.* **2016**, *98*, 113.

[5]   Y. Opoku-Damoah, R. N. Wang, J. P. Zhou, Y. Ding, *Theranostics* **2016**, *6*, 986.

[6]   S. Son, H. S. Min, D. G. You, B. S. Kim, I. C. Kwon, *Nano Today* **2014**, *9*, 525.

[7]   E. Kang, H. S. Min, J. Lee, M. H. Han, H. J. Ahn, I. C. Yoon, K. Choi, K. Kim, K. Park, I. C. Kwon, *Angew. Chem.* **2010**, *49*, 524.

[8]   M. A. Malvindi, A. Greco, F. Conversano, A. Figuerola, M. Corti, M. Bonora, A. Lascialfari, H. A. Doumari, M. Moscardini, R. Cingolani, G. Gigli, S. Casciaro, T. Pellegrino, A. Ragusa, *Adv. Funct. Mater.* **2011**, *21*, 2548.

[9]   T. H. Yin, P. Wang, R. Q. Zheng, B. Zheng, D. Cheng, X. L. Zhang, X.T. Shuai, *Int. J. Nanomed.* **2012**, *7*, 895.

[10] Z. H. Li, K. Dong, S. Huang, E. G. Ju, Z. Liu, M. L. Yin, J. S. Ren, X. G. Qu, *Adv. Funct. Mater.* **2014**, *24*, 3612.

[11] N. Teraphongphom, P. Chhour, J. R. Eisenbrey, P. C. Naha, W. R. T. Witschey, B. Opasanont, L. Jablonowski, D. P. Cormode, M. A. Wheatley, *Langmuir* **2015**, *31*, 11858.

[12] F. Yang, Y. X. Li, Z. P. Chen, Y. Zhang, J. R. Wu, N. Gu, *Biomaterials* **2009**, *30*, 3882.

[13] Z. Liu, T. Lammers, J. Ehling, S. Fokong, J. Bornemann, F. Kiessling, J. Gätjens, *Biomaterials* **2011**, *32*, 6155.

[14] F. Yang, Q. Wang, Z. X. Gu, K. Fang, G. Marriott, N. Gu, *ACS Appl. Mater. Interfaces* **2013**, *5*, 9217.

[15] S. Song, H. Guo, Z. Jiang, Y. Jin, Y. Wu, X. An, Z. F. Zhang, K. Sun, H. J. Dou, *Acta Biomater.* **2015**, *24*, 266.

[16] S. J. Xu, F. Yang, X. Zhou, Y. P. Zhuang, B. X. Liu, Y. Mu, X. Wang, H. Shen, G. Zhi, D. C. Wu, *ACS Appl. Mater. Interfaces* **2015**, *7*, 20460.

[17] K. Kooiman, H. J. Vos, M. Versluis, N. D. Jong, *Adv. Drug Delivery Rev.* **2014**, *72*, 28.

[18] S. Fokong, B. Theek, Z. J. Wu, P. Koczera, L. Appold, S. Jorge, U. R. Genger, M. V. Zandvoort , G. Storm, F. Kiessling, T. Lammers, *J. Controlled Release* **2012**, *163*, 75.

[19] H. Mannell, J. Pircher, F. Fochler, Y. Stampnik, T. Räthel, B. Gleich, C. Plank, O. Mykhaylyk, C. Dahmani, M. Wörnle, A. Ribeiro, U. Pohl, F. Krötz, *Nanomedicine* **2012**, *8*, 1309.

[20] C. C. Niu, Z. G. Wang, G. M. Lu, T. M. Krupka, Y. Sun, Y. F. You, W. X. Song, H. T. Ran, P. Li, Y. Y. Zheng, *Biomaterials* **2013**, *34*, 2307.

[21] H. Y. Huang, H. L. Liu, P. H. Hsu, C. S. Chiang, C. H. Tsai, H. S. Chi, S. Y. Chen, Y. Y. Chen, *Adv. Mater.* **2015**, *27*, 655.

[22] E. Y. Lukianova-Hleb, X. Y. Ren, R. R. Sawant, X. W. Wu, V. P. Torchilin, D. O. Lapotko, *Nat. Med.* **2014**, *20*, 778.

[23] W. B. Cai, H. L. Yang, J. Zhang, J. K. Yin, Y. L. Yang, L. J. Yuan, L. Zhang, Y. Y. Duan, *Sci. Rep.* **2015**, *5*, 13725.

[24] J. Y. Lee, D. Carugo, C. Crake, J. Owen, M. S. Victor, A. Seth, C. Coussios, E. Stride, *Adv. Mater.* **2015**, *27*, 5484.

[25] Y. J. Zhao, W. X. Song, D. Wang, H. T. Ran, R. H. Wang, Y. Z. Yao, Z. G. Wang, Y. Y. Zheng, P. Li, *ACS Appl. Mater. Interfaces* **2015**, *7*, 14231.

[26] T. Lammers, P. Koczera, S. Fokong, F. Gremse, J. Ehling, M. Vogt, A. Pich, G. Storm, M. V. Zandvoort, F. Kiessling, *Adv. Funct. Mater.* **2015**, *25*, 36.

[27] W. He, F. Yang, Y. H. Wu, S. Wen, P. Chen, Y. Zhang, N. Gu, *Mater. Lett.* **2012**, *68*, 64.

[28] L. Duan, F. Yang, L. N. Song, K. Fang, J. L. Tian, Y. J. Liang, M. X. Li, N. Xu, Z. D. Chen, Y. Zhang, N. Gu, *Soft Matter* **2015**, *11*, 5492.

[29] L. Cao, P. Du, S. H. Jiang, G. H. Jin, Q. L. Huang, Z. C. Hua, *Mol. Cancer Ther.* **2008**, *7*, 851.

[30] E. Chiellini, A. Corti, S. D'Antone, R. Solaro, *Prog. Polym. Sci.* **2003**, *6*, 963.

[31] M. H. Alves, B. E. B. Jensen, A. A. A. Smith, A. N. Zelikin, *Macromol. Biosci.* **2011**, *11*, 1293.

[32] J. Bzyl, M. Palmowski, A. Rix, S. Arns, J. M. Hyvelin, S. Pochon, J. Ehling, S. Schrading, F. Kiessling, W. Lederle, *Eur. Radiol.* **2013**, *23*, 468.

[33] Y. Negishi, N. Hamano, Y. Tsunoda, Y. Oda, B. Choijamts, Y. Endo-Takahashi, D. Omata, R. Suzuki, K. Maruyama, M. Nomizu, M. Emoto, Y. Aramaki, *Biomaterials* **2013**, *34*, 501.

[34] F. Kiessling, S. Fokong, J. Bzyl, W. Lederle, M. Palmowski, T. Lammers, *Adv. Drug Delivery Rev.* **2014**, *72*, 15.

[35] W. Cui, S. Tavri, M. J. Benchimol, M. Itani, E. S. Olson, H. Zhang, M. Decyk, R. G. Ramirez, C. V. Barback, Y. Kono, R. F. Mattrey, *Biomaterials* **2013**, *34*, 4926.

[36] Y. C. Chen, C. F. Chiang, S. K. Wu, L. F. Chen, W. Y. Hsieh, W. L. Lin, *J. Controlled Release* **2015**, *211*, 53.

[37] X. Wang, D. C. Niu, P. Li, Q. Wu, X. W. Bo, B. J. Liu, S. Bao, T. Su, H. X. Xu, Q. G. Wang, *ACS Nano* **2015**, *9*, 5646.

[38] A. E. F. Kruyt, *Cancer Lett.* **2008**, *1*, 14.

[39] M. Ma, Y. Zhang, W. Yu, H. Shen, H. Zhang, N. Gu, *Colloids Surf., A* **2003**, *212*, 219.

[40] C. A. Sennoga, V. Mahue, J. Loughran, J. Casey, J. M. Seddon, M. Tang, R. J. Eckersley, *Ultrasound Med. Biol.* **2010**, *36*, 2093.

[41] A. E. Harvey, J. A. Smart, E. S. Amis, *Anal. Chem.* **1955**, *27*, 26.